
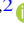




Evolution of the Progenitors of SNe 1993J and 2011dh Revealed through Late-time Radio and X-Ray Studies

E. Kundu^{1,2} , P. Lundqvist^{1,2} , E. Sorokina^{3,4}, M. A. Pérez-Torres^{5,9}, S. Blinnikov^{4,6,7}, E. O'Connor^{1,2}, M. Ergon^{1,2}, P. Chandra^{1,8}, and B. Das⁸

¹ Department of Astronomy, AlbaNova, Stockholm University, SE-10691 Stockholm, Sweden; esha.kundu@astro.su.se

² The Oskar Klein Centre, AlbaNova, SE-10691 Stockholm, Sweden

³ Sternberg Astronomical Institute, M.V. Lomonosov Moscow State University, Universitetski pr. 13, 119234 Moscow, Russia

⁴ Institute for Theoretical and Experimental Physics (ITEP), Moscow, Russia

⁵ Instituto de Astrofísica de Andalucía, Glorieta de las Astronomía, s/n, E-18008 Granada, Spain

⁶ Kavli Institute for the Physics and Mathematics of the Universe (WPI), University of Tokyo, Tokyo, Japan

⁷ All-Russia Research Institute of Automatics (VNIIA), Moscow, Russia

⁸ National Centre for Radio Astronomy, Tata Institute of Fundamental Research, Pune University Campus, Pune-411007, India

Received 2018 October 11; revised 2019 March 5; accepted 2019 March 5; published 2019 April 9

Abstract

We perform hydrodynamical simulations of the interaction between supernova (SN) ejecta and circumstellar medium (CSM) for SN 1993J and SN 2011dh, and calculate the radio and X-ray emissions expected from the shocked gas at late epochs (t). Considering the ejecta structure from multi-group radiation hydrodynamics simulation, we find that the observed rapid drop in radio and X-ray light curves of SN 1993J at $t > 3000$ days may be due to a change in the mass-loss rate (\dot{M}) ~ 6500 yr prior to the explosion of the SN. The exact epoch scales inversely with the assumed wind velocity of $v_w = 10$ km s⁻¹. The progenitor of this SN very likely belonged to a binary system, where, during its evolution, the primary had transferred material to the secondary. It is argued in this paper that the change in \dot{M} can happen because of a change in the mass accretion efficiency (η) of the companion star. It is possible that before ~ 6500 ($v_w/10$ km s⁻¹)⁻¹ yr prior to the explosion, η was high, and thus the CSM was tenuous, which causes the late-time downturn in fluxes. In the case of SN 2011dh, the late-time evolution is found to be consistent with a wind medium with $\dot{M}/v_w = 4 \times 10^{-6} M_\odot$ yr⁻¹/10 km s⁻¹. It is difficult from our analysis to predict whether the progenitor of this SN had a binary companion; however, if future observations show a similar decrease in radio and X-ray fluxes, then this would give strong support to a scenario where both SNe had undergone a similar kind of binary evolution before explosion.

Key words: circumstellar matter – hydrodynamics – radiation mechanisms: non-thermal – radiation mechanisms: thermal – supernovae: individual (SN 1993J, SN 2011dh)

1. Introduction

Supernovae (SNe) are the massive destruction of stars. The evolution of these stars before explosion depends on whether or not the star had interacted with a companion star during its lifetime (Podsiadlowski et al. 1992; Podsiadlowski 2001). In most cases, it is not possible to verify if the exploded star was part of a binary system, due to the large astronomical distances. However, indirect evidence, such as signs of hydrogen emission at early time and He I absorption at late epochs, or no trace of hydrogen line in the optical spectra, point toward a progenitor that has been stripped of most of, or the entire envelope because of an interaction with a secondary star (Nomoto et al. 1993; Podsiadlowski et al. 1993). Nevertheless, massive stars, with a main-sequence mass $> 20 M_\odot$, in isolation, can undergo huge mass-loss that is driven by strong winds (Schaller et al. 1992; Vink & Koter 2005) and periodic eruptions (Smith & Owocki 2006). This may partially or completely remove the very outermost layer. However, models suggest that stars that end their lives with very low envelope mass fall within a very narrow initial mass range (see Smartt 2015 for a review of missing high mass progenitors). Furthermore, the stripped envelope SN rate is not consistent with the fraction of massive single-stars that are expected to be accounted for in this kind of

SNe. Therefore, it is more probable that the majority of the stripped envelope progenitors are low mass stars and must originate from a binary system (Smith et al. 2011). In this case, during the evolution, the primary fills its Roche lobe and transfers material to the companion. It is found that the Roche lobe overflow is an effective mechanism through which stars can lose most of their envelope mass (Podsiadlowski et al. 1992; Podsiadlowski 2001). Stripped envelope SNe that display their optical spectra hydrogen lines at early epoch and a few weeks/months after the He I absorption feature are categorized as SN type IIb (see the review by Filippenko 1997).

In addition to SN 2008ax (Crockett et al. 2008) and SN 2013df (Van Dyk et al. 2014), the two other SNe IIb whose progenitor stars have been directly identified by analyzing the pre-explosion archival images are SN 1993J (Cohen et al. 1995) and SN 2011dh (Van Dyk et al. 2011). For SN 1993J, the optical light curve acquired just after the explosion revealed the presence of two peaks, which were best explained by a binary model with both stars having a mass of $\sim 15 M_\odot$ (Nomoto et al. 1993; Podsiadlowski et al. 1993). This scenario is further confirmed by Aldering et al. (1994), who studied the observed photometry of the SN. These authors concluded that the progenitor star was a G8-K0 supergiant. Furthermore, by investigating the ultraviolet images taken using the *Hubble Space telescope* (*HST*), Maund et al. (2004) justified the presence of a hot B type companion star in the vicinity of the SN. Later, Fox et al. (2014) drew a similar conclusion from

⁹ Visiting Scientist: Departamento de Física Teórica, Facultad de Ciencias, Universidad de Zaragoza, Spain.

the observations carried out at the far-ultraviolet spectral region. It is true that the companion of SN 1993J has so far avoided the discovery but it is almost certain that the progenitor of this SN was part of a binary system. In the case of SN 2011dh, a yellow supergiant (YSG) star was detected at the location of the SN by examining the pre-explosion *HST* archival images (Van Dyk et al. 2011). Initially, this star was thought to be either the binary companion of the SN or an unrelated star (Arcavi et al. 2011; Van Dyk et al. 2011; Soderberg et al. 2012) because the putative progenitor was found to be less extended compared to the detected YSG. However, using pre- and post-explosion *HST* and Gemini images, Maund et al. (2011), Van Dyk et al. (2013) established the fact that the YSG was the progenitor of SN 2011dh. The early-spectra of SN 2011dh has shown the presence of a thin layer of envelope (Arcavi et al. 2011; Marion et al. 2011) at the time of the explosion. Therefore, it could be expected that the progenitor of this SN belonged to a binary system. However, it has not been fully ruled out that it was instead the explosion of a star that had evolved in isolation (Georgy 2011).

In this regard, the medium surrounding SNe 1993J and 2011dh provides important clues about the evolution of both SNe. In a binary system, the primary usually transfers mass to the secondary through Roche lobe overflow. According to the accretion efficiency some fraction of this mass gets lost into the ambient medium. After the explosion, the supersonic SN ejecta interact with this medium and shocks are formed. These shocks channel part of their kinetic energy to accelerate charged particles into relativistic particles. As magnetic fields also get amplified in the shocks (Bykov et al. 2013; Caprioli & Spitkovsky 2014b; Kundu et al. 2017), these accelerated particles, mainly electrons, lose a fraction of their energy through synchrotron emission. This radiation often makes the SN shocks bright in radio frequencies. The intensity of this brightness depends on the density of the CSM, which means that the mass-loss history of the progenitor system can be mapped by studying this emission and hence we can gain information about the system. The X-ray emission at late epoch mainly comes from the shocked ejecta behind the reverse shock. Several mechanism (e.g., free-free, free-bound, two-photons, line emissions) contribute to the emission at late-times and provide important clues about the circumbinary medium.

The radio and X-ray observations of SN 1993J have revealed a sudden downturn in radio and X-ray fluxes beyond ~ 3000 days. In this paper, we study the evolution of the radio and the X-ray fluxes, from this SN by performing hydrodynamic simulations of the interaction of the SN ejecta with CSM and calculating the fluxes using a post-processing procedure. Given that SN 2011dh is similar to SN 1993J in many aspects, a similar analysis has been carried out for this SN.

Along with the CSM, the SN ejecta structure plays an important role in the evolution of the SN. Therefore, we considered the ejecta structure of SN 1993J and SN 2011dh from numerical simulations that use multi-group radiation hydrodynamic simulations (STELLA) to evaluate the structures. The details of the STELLA simulations and the ejecta structure are discussed in detail in Section 2. The rest of the paper is arranged as follows. In Section 3, we present the hydrodynamical simulations of the interaction between the SN ejecta and the CSM. Afterwards, Sections 4–6 give an account of radio and X-ray data, and modeling of radio and X-ray emission, respectively. The results are presented and discussed

in Sections 7 and 8, respectively. Finally, we draw our conclusions in Section 9.

2. Ejecta Model

The ejecta profiles that we use in our simulations are taken from STELLA, which is a multi-group radiation hydrodynamics code (Blinnikov et al. 1998, 2000, 2006). The ejecta structures at day 1 after the explosion are shown in solid lines in Figure 1, which are re-scaled, considering homologous expansion, from the ejecta profiles calculated at 490 and 462 days after the outbursts of SN 1993J and SN 2011dh, respectively. The stellar model considered in STELLA for SN 1993J and SN 2011dh are the re-mapped models 13C of Woosley et al. (1994) and 13Cdh, respectively. The remapping procedure for the STELLA grid is described in Blinnikov et al. (1998). The models were brought to the static equilibrium while preserving a $P(\rho)$ structure identical to that of the original model 13C, and keeping the total mass and the chemical composition for both models identical to 13C. Here, P and ρ represent pressure and density, respectively. 13Cdh is derived from the 13C of Woosley et al. (1994), where the radius of the pre-supernova star has been re-scaled to match the faster and weaker shock breakout maximum of SN 2011dh. The explosion energy of SN 2011dh that allows us to fit the observations is 2×10^{51} erg, which is a little larger than that of SN 1993J. The details of the model and the multicolor light curves are compared to the observations of SN 2011dh in Tsvetkov et al. (2012). Model 13C is a binary model in which the primary, with a main-sequence mass of $13 M_{\odot}$, has lost most of its hydrogen envelope to a nearby companion star of mass $9 M_{\odot}$. The initial separation between the two stars was 4.5 au. As the primary undergoes large mass-loss because of strong interaction with the secondary, around $0.2 M_{\odot}$ of the hydrogen envelope is left just before explosion. The pre-supernova star has a radius of 4.33×10^{13} cm and the core, which is composed of helium and heavy elements, has a mass of $3.71 M_{\odot}$. It is interesting to note that the density structure here is different from what is shown in Figures 3 and 4 by Blinnikov et al. (1998) for age 1 day after the explosion. This is a good illustration to the absence of the fully homologous expansion stage of the evolution for the SNe with a region of ^{56}Ni inside. The thermalization of gamma-photons from ^{56}Ni to ^{56}Co to ^{56}Fe decays leads to the formation of a hot bubble with a depressed density, which causes the formation of additional shocks and continues to change the gas distribution along the ejecta during several weeks after the explosion. The comparison between the hydrodynamical structure provided by radiation-hydrodynamical calculations and the Monte-Carlo calculations was discussed in Woosley et al. (2007). For the present work, the details of $\rho(v)$ distribution also can be important, where v represents velocity.

3. Hydrodynamical Simulation

It is often assumed that the interaction between SN ejecta and CSM can be described by a self-similar structure (Chevalier 1982). This is a reasonable approximation if the outer part of the ejecta and CSM both have a power-law density profile, and the ejecta density profile is not too shallow. However, from multi-group radiation hydrodynamics simulation (e.g., STELLA) of an exploded star, there is evidence that the density of the outer part of a SN can differ from a power-law structure. In this case, the evolution of the SN can no

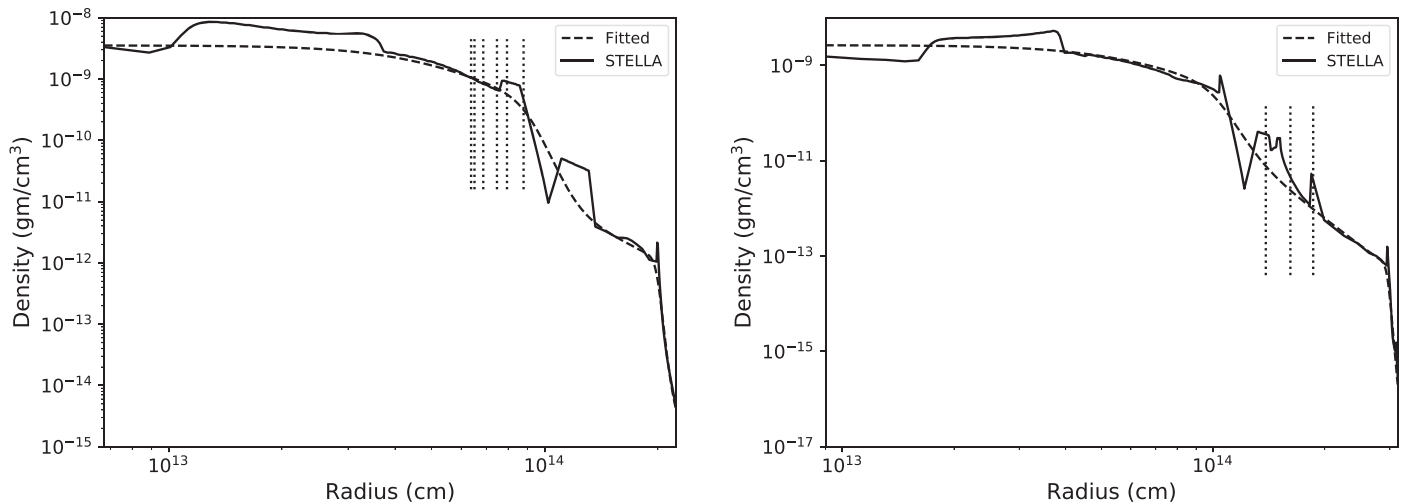


Figure 1. Ejecta structure of SN 1993J (left-hand panel) and SN 2011dh (right-hand panel) at day 1 after the explosion of respective supernovae from STELLA. The fitted ejecta profiles are shown in dashed lines. The dotted line from right to left display the positions of the reverse shock in the ejecta at 1000, 2000, 3000, 5000, 7000 and 8000 days since the explosion of SN 1993J (left-hand panel) and at 200, 500 and 1200 days after the explosion of SN 2011dh (right-hand panel).

longer be approximated by a self-similar solution and one needs hydrodynamical simulations to estimate the structure.

As displayed in Figure 1 (in solid lines), the ejecta profiles of both SNe 1993J and 2011dh, as estimated from STELLA, are quite complicated. Therefore, we evaluate the shock structure by performing hydrodynamical simulation of SN and CSM interaction. To do the simulation, we use the publicly available FLASH code, the Radiation Blast Wave problem, which has been modified accordingly to meet our requirements. FLASH (Fryxell et al. 2000)¹⁰ is a parallel, hydrodynamical code that is written in Fortran 90 and C. The hydrodynamical modules implemented here assume that the flow can be described by the Euler equations for compressible gas. The hydro unit is inherited from the PROMETHEUS code (Fryxell et al. 1989) and uses the split Piecewise-parabolic Method (PPM). The PPM is described in detail in Colella & Woodward (1984). To solve the Euler equations numerically, a Riemann solver, known as the Harten, Lax and van Leer solver (Harten et al. 1983), is called in our simulations. We use a Courant–Friedrichs–Lewy (CFL) value of 0.6 for these runs.

The original radiation blast wave problem consists of a gas that is initially at rest and has a constant density. The temperature of the gas and radiation are not same inside a sphere of radius R_{int} , which is centered at the origin. However, they are in thermal equilibrium beyond R_{int} . In our case, the gas is made up of 63% hydrogen and 37% helium (by mole fraction) and obeys the ideal gas law, with an adiabatic index 5/3. Radiation is not included in our simulations. The temperature of the gas is 100 K and the density profile is a combination of the density structures of SN ejecta and CSM. In Figure 1 the density of the ejecta, at day 1 after the explosion, are shown for both SN 1993J (left-hand panel) and SN 2011dh (right-hand panel). The radius of the ejecta at this epoch is $R_{\text{int}} \equiv 2.24 \times 10^{14}$ cm (3.15×10^{14} cm) for SN 1993J (SN 2011dh). We assume that our SNe start to interact with the ambient media one day after the stars go off. Therefore, in our simulation, the input density consists of the density profile of ejecta (ρ_{ej}) up to a radius R_{int} , and beyond this the density profile is given by the CSM (ρ_{csm}) such that at day 1, just prior to the

interaction, $\rho_{\text{ej}}(R_{\text{int}}) = \rho_{\text{csm}}(R_{\text{int}})$. For SN 1993J (SN 2011dh) the density structures of CSM is given by Equation (14) (winds; see Section 7.1.2 for details). The STELLA outputs, i.e., the ejecta structures are fitted with analytic functions to make the initial conditions smooth. These analytic fits to the ejecta structures are shown in dashed lines in Figure 1.

The simulations are performed in one-dimension considering spherical geometry. The computational domain for SN 1993J and SN 2011dh are $0 \text{ cm} < r < 3 \times 10^{18} \text{ cm}$ and $0 \text{ cm} < r < 1 \times 10^{18} \text{ cm}$, respectively, where r represents radius. We use a uniform grid, where each cell has a width of 2.13×10^{12} cm (6.51×10^{11} cm) for SN 1993J (SN 2011dh). The interaction of the supersonic SN ejecta with the almost stationary CSM launches two shocks: one shock moves forward into the CSM, hence called the forward shock, while the other shock recedes into the ejecta in mass coordinate, and is known as the reverse shock. We run our FLASH simulations until 8000 days (3000 days) after the explosion of SN 1993J (SN 2011dh). The FLASH output of the density profile of the entire simulation, including both of the expanding unshocked SN ejecta and CSM, is shown in Figure 2 at 2000 days past explosion of SN 1993J. A zoom in on the morphology of the density, velocity, temperature and pressure across the shocked region is shown in Figure 3. To highlight the evolution, the density and temperature profiles of the shocked gas at 1000, 2000, 4000 and 8000 days after explosion of SN 1993J are displayed in Figure 4. Here, solid lines represent the density. In computing the evolution of the shocks, no radiative cooling was included in the hydro code. Cooling is chiefly important at early epochs when the density of the shocked gas is higher, and inverse Compton (IC) scattering in the region close to the forward shock plays a role. Therefore, these processes will mainly affect the evolution at early epochs (Fransson et al. 1996). At late time, radiative cooling will only have an insignificant effect; as discussed in Section 7.2. Of potentially greater importance is that we have assumed full equipartition between electrons and ions. In reality, the electron temperature may be lower than the ion temperatures of the shocked gas. We discuss this point further in Section 7.2.

¹⁰ Also see the FLASH manual at http://flash.uchicago.edu/site/flashcode/user_support/flash4 Ug_4p4.pdf.

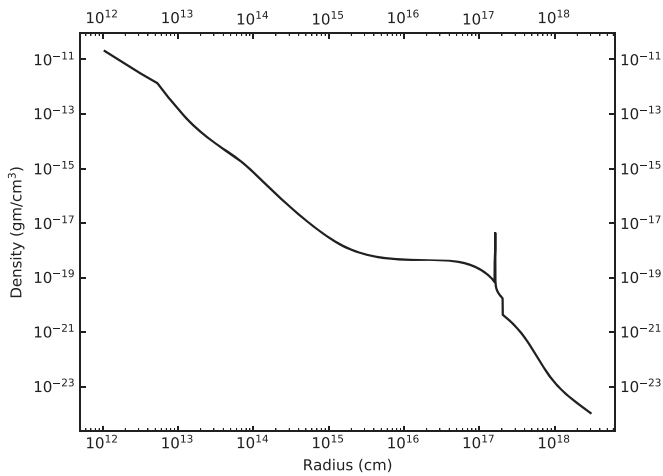


Figure 2. Density profile of the expanding SN ejecta with the shocked gas and unshocked CSM post 2000 days since the explosion of SN 1993J. Note the steep slope in the unshocked CSM beyond 2×10^{17} cm, which then rolls off to an r^{-2} wind at $r \geq 2 \times 10^{18}$ cm.

4. Radio and X-Ray Data

In this paper, for SN 1993J, we have modeled the post-1000 days radio data that was published in Weiler et al. (2007) (for details see the references therein), Dwarkadas et al. (2014), and also that presented in B. Das et al. (2019, in preparation). Meanwhile, for the X-ray modeling we used data from Chandra et al. (2009). Furthermore, for completeness, we include the X-ray data presented in Dwarkadas et al. (2014). Given that we are interested in modeling the late time emissions from both SNe, for SN 2011dh, we compare our model’s prediction with the X-ray observation carried out ~ 500 days after the explosion (Maeda et al. 2014). For radio, we reanalyzed the publicly available data taken with the Karl G. Jansky Very Large Array (VLA¹¹), from the surroundings of SN 2011dh, taken on 2012 August 1, 2014 January 31 and 2014 October 18. In addition, data published in Soderberg et al. (2012), Krauss et al. (2012) and de Witt et al. (2016) are considered to model the radio emission. The distances to SN 1993J and SN 2011dh considered in our study are 3.63 Mpc (Freedman et al. 1994) and 8.4 Mpc (Feldmeier et al. 1997), respectively.

The observations presented here were obtained as part of the VLA programs 12A-286, 13A-370, and 14A-479. We processed and imaged the data using the Common Astronomy Software Application (CASA) software package (McMullin et al. 2007). The source 3C286 was used in all three observing runs for bandpass and absolute flux density calibration purposes, for all frequencies and epochs. For phase calibration purposes, the sources J1335+4542, J1327+4326, and J1349+5341 were used for the 2002 August 1, 2014 January 31, and 2014 October 18 observations. Our results are summarized in Table 1, and in Figure 5. We note that our 8.4 GHz data point for our 2014 January 31 (PI: Arcavi) epoch indicates a flux density about three times smaller than the flux density published by de Witt et al. (2016). Since this large difference in flux density has a correspondingly large impact in the radio light curve and its physical interpretation, we carefully reanalyzed all three datasets, particularly the data for 2014

January 31, because there were many sources in the field surrounding the SN. After this procedure, we confirmed that the source position for the VLA source that we identify with SN 2011dh in both 2014 January 31 and October 18, which agrees within about 1 milliarcsecond with the VLBI position of SN 2011dh published by Martí-Vidal et al. (2011b) and with the position published by de Witt et al. (2016). We note that there is a source northwards of the actual SN 2011dh, which has a flux density of about $600 \mu\text{Jy}/\text{beam}$; i.e., about three times larger than SN 2011dh. We also notice that the observations of 2014 October 18 (PI: Arcavi) were phase-centered to a position significantly off the SN discovery position. Therefore, we suspect that de Witt et al. (2016) might have been confused by that source northern of the SN, which is about 10 times brighter than the actual radio luminosity of SN 2011dh for this epoch.

The broadband VLA data displayed in Figure 5 shows three different epochs, and an inverted spectral behavior at frequencies ≥ 5.0 GHz both in 2014 January and October.

5. Radio Emission

The radio emission originates from the shocked gas enclosed between the reverse and the forward shocks. The forward shock interacts with the immediate surrounding medium and accelerates the charged particles in the ambient medium in relativistic energies. These shocks are also ideal places where effective magnetic field amplification takes place (Bykov et al. 2013; Caprioli & Spitkovsky 2014a, 2014b; Kundu et al. 2017). In the presence of the magnetic field, the shock accelerated charged particles emit part of their energy as synchrotron radiation in the radio wavelengths. According to diffusive acceleration theory, the energy distribution of the accelerated particles follows a power-law profile; i.e., $dN/dE = N_0 E^{-p}$, where N_0 and E are the normalization constant and particle energy, respectively; p represents the power-law index. It is very likely that the seed particles acquire a certain percentage of the post-shock energy during the acceleration process. Because electrons over ions are expected to be the main source of radio emission in SNe, we assume that all of the electrons are accelerated in the post-shock region and that a constant fraction of post-shock energy, ϵ_e , gets channeled into them. Here $\epsilon_e = u_e/u_{\text{th}}$, where u_e represents the energy density of electrons. $u_{\text{th}} = 9/8 \rho_{\text{csm}}(r) v_s^2$ is the post-shock thermal energy density, with v_s representing the shock speed. As for electrons, we presume that the fraction of post-shock kinetic energy that is converted into magnetic field is $\epsilon_B = u_B/u_{\text{th}}$, where u_B is the energy density of the magnetic field. In modeling the radio emission, it is surmised that the emission is coming from a spherical homogeneous shell. Therefore, considering synchrotron self-absorption (SSA) and external free-free absorption as the dominating absorption mechanisms, the optically thin luminosity of this radiation, due to relativistic shock accelerated electrons with a power-law index of p , from a shell having an outer radius and thickness of r_s and Δr , respectively, can be written as

$$L_{\nu, \text{thin}} = \frac{8\pi^2 k_B T_{\text{bright}} \vartheta_\nu r_s^2}{c^2 f \left(\frac{\nu_{\text{peak}}}{\nu_{\text{abs}}} \right)} \nu_{\text{abs},0}^{(p+3)/2} \nu^{-(p-1)/2} \exp[-\tau_{\text{ff}}(r_s)], \quad (1)$$

¹¹ The VLA is operated by the National Radio Astronomy Observatory, a facility of the National Science Foundation operated under cooperative agreement by Associated Universities, Inc.

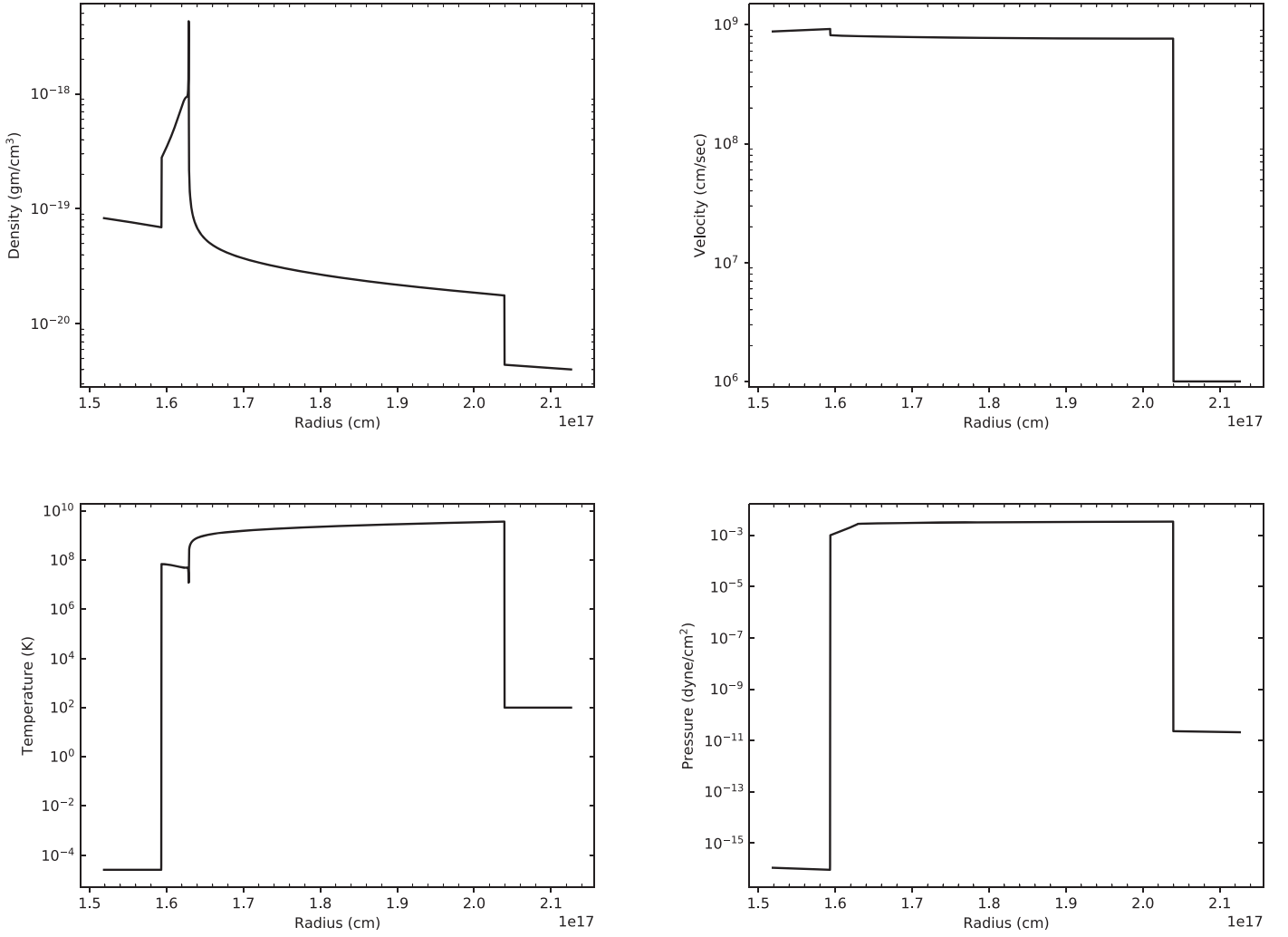


Figure 3. Morphology of density (upper left-hand panel), velocity (upper right-hand panel), temperature (lower left-hand panel) and pressure (lower right-hand panel) across the shocked region at 2000 days post the explosion of SN 1993J.

with

$$\nu_{\text{abs},0} = (2\Delta r \kappa(p) N_0 B^{(p+2)/2})^{2/(p+4)}, \quad (2)$$

and

$$f(x) = x^{1/2}[1 - \exp(-x^{-(p+4)/2})], \quad (3)$$

where T_{bright} is the brightness temperature. $\vartheta_\nu = \frac{L_\nu}{L_{\nu,0}}$ with $L_{\nu,0} = 4\pi^2 r_s^2 I_\nu(0)$; $I_\nu(0)$ is the intensity of radiation along the line of sight for which the path length of the radiation is equal to the thickness of the shock; ν_{peak} is the peak frequency of radiation; τ_{ff} is the free-free optical depth; B represents magnetic field strength and $\kappa(p)$ is the SSA coefficient; and k_B and c represent the Boltzmann constant and speed of light in vacuum, respectively.

For SN 1993J, we have assumed a CSM out to 2×10^{17} cm, which is characterized by a mass-loss rate of \dot{M} , of $4 \times 10^{-5} M_\odot \text{ yr}^{-1}$ and a wind velocity $v_w = 10 \text{ km s}^{-1}$. For such a high mass-loss rate, radio emission from this SN could suffer from external free-free absorption. We assume that the ambient media of both SNe, SN 1993J and SN 2011dh, are made up of hydrogen and helium, with solar abundances, and that it is completely ionized due to strong UV radiation from shock breakout and X-ray emission from forward and reverse shocks

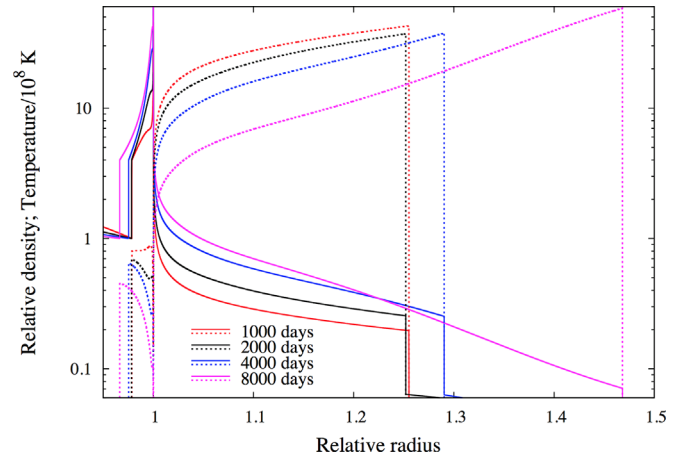


Figure 4. Density (solid lines) and temperature (dotted lines) profiles across the shocked region at 1000, 2000, 4000 and 8000 days past the explosion of SN 1993J. Note the inflated region of shocked CSM at the latest epoch, and the increasing shock temperature with time of the forward shock.

(Fransson et al. 1996). If the number density of hydrogen and helium in the surrounding medium are $n_{\text{H}}(r)$ and $n_{\text{He}}(r)$, respectively, then the absorption coefficient due to free-free is

Table 1

Karl G. Jansky Very Large Array Radio Observations of SN 2011dh

Epoch yyyy mm dd	Day since Explosion days	Frequency (GHz)	Flux Density (μ Jy)
2012 Aug 1	428	8.4	880 ± 60
		8.55	778 ± 24
		9.56	663 ± 23
		13.50	507 ± 17
		14.50	466 ± 17
2014 Jan 31	976	4.74	132 ± 6
		5.26	115 ± 8
		6.84	83 ± 9
		7.36	108 ± 3
		8.4	180 ± 20
		8.42	61 ± 6
2014 Oct 18	1236	4.67	53 ± 5
		4.93	46 ± 9
		5.18	42 ± 14
		7.02	53 ± 8
		7.72	72 ± 5
		8.4	95 ± 20
		18.49	65 ± 25
		19.51	30 ± 21
		20.49	35 ± 11
		21.51	30 ± 18
		22.49	44 ± 17
		23.51	97 ± 38
		24.49	39 ± 24
25.51	36 ± 26		

given by

$$\alpha_{\text{ff}}(r) = 0.018 T_{\text{csm}}^{-3/2} \frac{n_e^2(r)}{1 + 2y} \nu^{-2} [\bar{g}_{\text{ff}}^{\text{H}}(T_{\text{csm}}, \nu) + 4y \bar{g}_{\text{ff}}^{\text{He}}(T_{\text{csm}}, \nu)] \text{ cm}^{-1}, \quad (4)$$

where T_{csm} is the temperature of the CSM. Here $n_e(r)$ represents the number density of the electron in the ambient medium and $y = n_{\text{He}}(r)/n_{\text{H}}(r)$. $\bar{g}_{\text{ff}}^{\text{H}}(T_{\text{csm}}, \nu)$ and $\bar{g}_{\text{ff}}^{\text{He}}(T_{\text{csm}}, \nu)$ are the velocity average Gaunt factors for hydrogen and helium, respectively. In case of SN 1993J, the temperature of the CSM is $\sim 10^5$ K (Björnsson & Lundqvist 2014). For radiation in GHz frequency and $T_{\text{csm}} < 3 \times 10^5 z^2$, $\bar{g}_{\text{ff}}(T_{\text{csm}}, \nu) = \frac{\sqrt{3}}{\pi} \left(17.7 + \log \left(\frac{T_{\text{csm}}^{1.5}}{z\nu} \right) \right)$, where z is the atomic number of a given element, while for $T_{\text{csm}} > 3 \times 10^5 z^2$ the Gaunt factor is given as $\bar{g}_{\text{ff}}(T_{\text{csm}}, \nu) = \frac{\sqrt{3}}{\pi} \log \left(\frac{2.2kT_{\text{csm}}}{h\nu} \right)$ (Tucker 1975). In the case of a wind medium, which extends up to a radius $r \gg r_s$, τ_{ff} is written as

$$\tau_{\text{ff}}(r_s) = \frac{1}{3} r_s \alpha_{\text{ff}}(r_s). \quad (5)$$

However, if the density of ambient medium starts to decrease, or increase, beyond a given radius R_{chng} , then the free-free optical depth becomes

$$\tau_{\text{ff}}(r_s) = \frac{1}{3} r_s \alpha_{\text{ff}}(r_s) (1 - f_{\text{Rchng}}^3 (1 - f_{\text{rate}}^2)), \quad (6)$$

where $f_{\text{Rchng}} = r_s/R_{\text{chng}}$ and $f_{\text{rate}} = \frac{\dot{M}^1/v_w^1}{\dot{M}/v_w}$. \dot{M}^1/v_w^1 is the ratio between the mass-loss rate and wind velocity, which characterize the medium at $r \geq R_{\text{chng}}$.

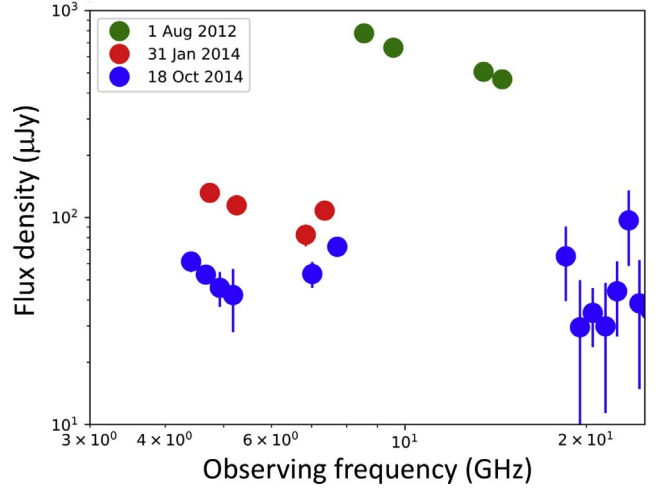


Figure 5. Broadband VLA radio spectra of SN 2011dh between 2012 and 2014.

6. X-Ray Emission

We modeled the X-ray emission at late epochs, when the shocked ejecta behind the reverse shock mainly contributes to this emission. The emission processes that we considered for our study are free-free, free-bound, two-photon and line emissions. In a medium where the external radiation is negligible, the ionization structure of the shocked ejecta can be calculated by balancing collisional ionization with direct and dielectronic recombination. For an element z , if X_m represents the ionization fraction of ionization stage m , then the rate of change of X_m can be written as

$$\frac{dX_m}{dt} = N_e [-(\beta_m + \mathcal{C}_m) X_m + \beta_{m+1} X_{m+1} + \mathcal{C}_{m-1} X_{m-1}], \quad (7)$$

(Nymark et al. 2006) where N_e is the number density of free electrons; β_m represents the recombination coefficient from the ionization state m to $m - 1$; and \mathcal{C}_m is the ionization rate from ionization state m to $m + 1$. We assumed steady state condition, i.e., $\frac{dX_m}{dt} = 0$, and solved the equation for each ionization stage of a given z . We also included an additional process, namely charge transfer. The elements included in our study to calculate the emission are H, He, C, N, O, Ne, Na, Mg, Al, Si, S, Ar, Ca, Fe and Ni.

In hot ejecta, free electrons can excite atoms/ions to higher energy states, which can subsequently decay by the emission of photons. Collisional de-excitation is also important when the density of free electrons is high enough. In this kind of medium, for an ionization state z_m of a given element, which is in an excitation level i , under equilibrium we write

$$\sum_{j \neq i} N(z_m)_j N_e q_{ji} + \sum_{j > i} N(z_m)_j A_{ji} = \sum_{j \neq i} N(z_m)_i N_e q_{ij} + \sum_{j < i} N(z_m)_i A_{ij}, \quad (8)$$

with

$$\sum_j N(z_m)_j = N(z_m), \quad (9)$$

and

$$q_{ij} = \int_0^\infty \mathbb{V} \sigma_{ij} f(\mathbb{V}) d\mathbb{V}. \quad (10)$$

Here $N(z_m)$ represents the density of ionization stage m of an element z ; A_{ij} and σ_{ij} are the transition probability and collisional cross section for the i to j transition, respectively; and $f(\mathbb{V})$ represents the thermal distribution of speed of free electrons with \mathbb{V} being the speed of electrons.

Recombination results in continuum free-bound emission, followed by a cascade of lines (Osterbrock 1989). For thermal electrons, the free-bound emission coefficient can be written as (Osterbrock 1989)

$$j_\nu^{fb} = \frac{1}{4\pi} N(z_m) N_e \sum_{n=n_1}^\infty \sum_{L=0}^{n-1} \mathbb{V} \sigma_{nL} f(\mathbb{V}) h\nu \frac{d\mathbb{V}}{d\nu}. \quad (11)$$

Here σ_{nL} and L represent the recombination cross section and orbital angular momentum, respectively; and h is the Planck constant.

Another continuum emission process is free-free emission, or bremsstrahlung. For isotropic thermal electrons that can scatter on an element z in an ionization state m , the emission coefficient for free-free radiation is given as (Rybicki & Lightman 1979; Osterbrock 1989)

$$j_\nu^{ff} = \frac{1}{4\pi} \frac{2^5 \pi e^6}{3 m_e c^3} \left(\frac{2\pi}{3 k_B m_e} \right)^{1/2} T^{-1/2} z^2 N(z_m) N_e \times \exp(-h\nu/k_B T) \bar{g}_{ff}(T, \nu), \quad (12)$$

where T and m_e represent the temperature and rest mass of the electrons, respectively; and e is the electric charge.

Continuum emission is also produced by two-photon decay because electrons populated in the 2^2S level can decay to 1^2S by the emission of two photons. The emission coefficient corresponding to this radiation is

$$j_\nu^{2\gamma} = \frac{1}{4\pi} N_{2^2S} A_{2^2S,1^2S} 2h \nu P(\nu), \quad (13)$$

(Osterbrock 1989) where, in each decay, $P(\nu)$ is the normalized probability for one photon to emit in the energy range ν_{12} and $(\nu + d\nu)\nu_{12}$; $h\nu_{12}$ is the energy difference between the two levels 1^2S and 2^2S ; and $A_{2^2S,1^2S}$ and N_{2^2S} represent the transition probability and density of electron in the 2^2S state, respectively.

To calculate the X-ray emission, we have post-processed the output data from the adiabatic hydrodynamic models. The total emissivity due the above-mentioned processes is calculated using a plasma code, which is described in some detail in Sorokina et al. (2004), and was also used in Mattila et al. (2008). It is assumed in our model that the plasma is in collisional equilibrium for a given electron temperature.

7. Results

Both SN 1993J and SN 2011dh have been followed extensively in radio and X-ray wavelengths (Pooley & Green 1993; Kohmura et al. 1994; van Dyk et al. 1994; Marcaide et al. 1995a, 1995b, 1997, 2009; Bartel et al. 2000, 2002; Immler et al. 2001; Pérez-Torres et al. 2001, 2002; Uno et al. 2002; Swartz et al. 2003; Zimmermann & Aschenbach 2003; Chandra et al. 2004, 2005, 2009; Weiler et al. 2007; Martí-Vidal et al. 2011a, 2011b; Bietenholz et al. 2012; Campana &

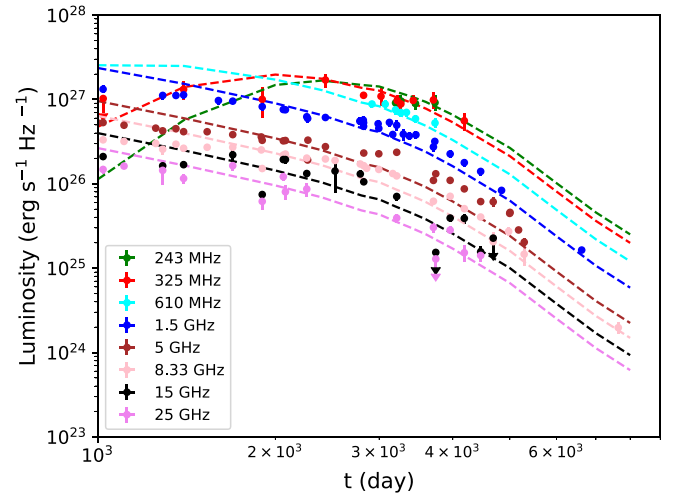


Figure 6. Modeled radio light curves of SN 1993J post-1000 days. The data are from Weiler et al. (2007), Dwarkadas et al. (2014) and Das et al. (2019, in preparation). The observed light curves show a sudden downturn in luminosity beyond ~ 3000 days. From our analysis, it is found that this drop is related to a rapid decrease in CSM density beyond a radius 2×10^{17} cm. The density of the ambient medium in our model is given by Equation (14). It is found that up to ~ 3000 days, the radio fluxes are consistent with a wind medium characterized by a \dot{M} of $4 \times 10^{-5} M_\odot \text{ yr}^{-1}$ and wind velocity of $v_w = 10 \text{ km s}^{-1}$.

Immler 2012; de Witt et al. 2016; Krauss et al. 2012; Soderberg et al. 2012; Maeda et al. 2014). Here, we have modeled the radio and X-ray emission at late stages, post-1000 days for the former and beyond ~ 100 days for the latter, to gain information about the evolution of the progenitor before explosion and also the structure of the SN ejecta.

7.1. Radio

7.1.1. SN 1993J

The radio light curves for SN 1993J at various frequencies are shown in Figure 6. The observed light curves show a sudden drop in flux beyond ~ 3000 days. To replicate the sudden downturn in flux, it has been argued that this indicates a rapid decrease in the density of the surrounding medium at the position of the forward shock at ~ 3000 days. It is also possible that this downturn is related to fact that the reverse shock ~ 3000 days post-outburst starts to invade into the flat inner ejecta. This will affect the evolution of the shocked gas encapsulated between the reverse and forward shock. For the \dot{M}/v_w that we have assumed and the explosion model that we have used, we do not find that the reverse shock encounters any drastic change in the density profile of the unshocked ejecta gas at around 3000 days.

From our analysis, it is found that the wind medium is extended up to a radius, R_{chng} , of 2×10^{17} cm. Beyond this, the density starts to drop rapidly. To reproduce the observed radio light curves beyond 1000 days, the density of the CSM in our model follows

$$\rho_{\text{csm}}(r) = \rho_{\text{csm}}^1(r) \left(0.05 + \frac{0.95}{1 + \left(\frac{r}{4 \times 10^{17} \text{ cm}} \right)^4} \right) \frac{\text{g}}{\text{cm}^{-3}}, \quad (14)$$

where $\rho_{\text{csm}}^1(r) = \dot{M}/4\pi r^2 v_w$ with $\dot{M} = 4 \times 10^{-5} M_\odot$ and $v_w = 10 \text{ km s}^{-1}$. The mass-loss rate and wind velocity considered in our model for $t < 3000$ days are similar to those required by

Fransson et al. (1996) and Fransson & Björnsson (1998) to model the radio and X-ray emissions at early epochs.

In Figure 2, the rapid drop in CSM density is visible at $r > 2 \times 10^{17}$ cm. Note that here we assume that the sudden drop in density continues up to a radius, R_{out} , 2×10^{18} cm, beyond which the CSM again attains a wind profile, as characterized by a mass-loss rate of $\dot{M}/20$ and $v_w = 10 \text{ km s}^{-1}$. The radio light curves computed from our model using an ambient medium given by Equation (14) are shown in dashed lines in Figure 6. As shown in the figure, our calculated radio fluxes at different frequencies can reproduce the observed downturn with reasonable accuracy. It should be noted that we did not include any local density fluctuations in the CSM in our model. These variations could be the reason of the local fluctuations seen in the data.

Very Long Baseline Interferometry (VLBI) images of SN1993J show that the radio emission comes from a nearly spherical shell (Marcaide et al. 1995a, 1995b, 1997; Bartel et al. 2000; Marcaide et al. 2009; Martí-Vidal et al. 2011b), whose shell width is estimated to be $\sim 31\%$ of the external radius (Marcaide et al. 2009; Martí-Vidal et al. 2011b). Therefore, in our calculation we assumed that for both SN 1993J and SN 2011dh the radiation comes from such a spherical shell. The evolution of this shell is calculated by performing hydrodynamical simulations, as described in Section 3. At any given epoch, the shell variables (e.g., the forward shock radius, velocity, density etc.) can be obtained from the simulations (see Figures 3 and 4). The shock variables required for our calculations are the radii of the forward shock (r_s) and the contact discontinuity (r_c), density of the shocked CSM ($\rho_{\text{sh, csm}}$), and the velocity of the forward shock (v_s). In the upper left-hand panel of Figure 3, the density spike on the left and the sharp discontinuity on the right side represent the position of r_c and r_s , respectively. We assume in our model (see Kundu et al. 2017 for details) that the radio emission comes from the region between r_c and r_s . Therefore, for us $\Delta r = r_s - r_c$. As displayed in Figures 3 and 4, there are variations in $\rho_{\text{sh, csm}}$ and v_s across Δr . Thus, to get average values of these variables we determine them at $r = r_c + \Delta r/2$. As can be seen in Figure 4, the density of the shocked CSM, except for close to r_c , is fairly constant with radius for the first few thousand days. Choosing parameters half-way through the shock is therefore not an important source of error. However, at 8000 days, there is a huge variation in density within the shocked CSM, consequently the error due to selecting representative parameters at this epoch is larger.

From spectral analysis, Weiler et al. (2007) found that both early and late epoch radio data are consistent with a spectral index of -0.8 . Therefore, the power-law index, p , of the electrons responsible for this emission is 2.6. We did our modeling considering this value for p and $T_{\text{bright}} = 3.6 \times 10^{10}$ K. Given that the radio source is expected to be homogeneous at late epochs, the assumption of a constant value for T_{bright} is reasonable. For other three parameters we assume $T_{\text{csm}} = 6 \times 10^5$ K and $\epsilon_e = \epsilon_B = 0.03$.

7.1.2. SN 2011dh

The light curves of SN 2011dh are shown in Figure 7. The left-hand panel shows the evolution of luminosity in the range 300 MHz–4.9 GHz while the right plot displays that between 6.7 GHz and 36 GHz. It is found from our analysis that for this SN the emission is consistent with a wind medium with a

$\dot{M}/v_w = 4 \times 10^{-6} M_{\odot} \text{ yr}^{-1}/10 \text{ km s}^{-1}$ until ~ 1300 days (or up to the time that archival data is available) since explosion. It is noted that our model predicts the low energy light curves (left-hand panel of Figure 7) with good accuracy, whereas the estimates are not that precise in the case of fluxes that are acquired at high frequencies (see the right-hand panel of Figure 7), especially at early epochs. The reason behind this discrepancy is that at high frequencies the emission becomes optically thin within a few days after the outbursts. IC loss plays a major role at early epoch, ~ 20 days after the explosion, which steepens the electron spectrum and hence the radio flux decreases. In our radio calculation, we have not considered the loss due to IC. Therefore, for high frequencies, we have overpredicted the fluxes at early epochs. Furthermore, radiative cooling is not included in our hydro-simulation. This is important at an early time, as described in Section 3, especially for SN 1993J.

For SN 2011dh, we assumed $p = 2.95$ (Krauss et al. 2012; Soderberg et al. 2012), $\epsilon_e = 0.03$ and $\epsilon_B = 0.04$. At early times, if the radio emission does not come from a homogeneous spherical shell, then the brightness temperature cannot be represented by a fixed temperature. It is found from our fitting that for SN 2011dh, $T_{\text{bright}} = 3.9 \times 10^9 (t/1 \text{ day})^{0.32}$ K for $t \leq 1500$ days. Beyond 1500 days, the source will have a brightness temperature of 4×10^{10} K. It is noted that for this SN we do not need to take into account free-free absorption while calculating the radio fluxes because the density of the CSM is low. The shock front radii and velocities predicted by our model at around 80 and 180 days after the explosion are found to be in good agreement with that estimated using the VLBI observations carried out at similar epochs (Bietenholz et al. 2012).

7.2. X-Rays

7.2.1. SN 1993J

For SN 1993J, X-ray data until 5408 days are compiled in Chandra et al. (2009). Additional data up to day ~ 7650 are plotted in Dwarkadas et al. (2014). All data are shown in Figure 8, together with our model results using the ejecta model described in Section 2 and a wind density characterized by $4 \times 10^{-5} (v_w/10 \text{ km s}^{-1}) M_{\odot} \text{ yr}^{-1}$; i.e., ten times higher circumstellar density than for our SN 2011dh simulations. Beyond a radius of $\sim 2 \times 10^{17}$ cm, we assume a steeper density profile in the circumstellar medium than $\rho_w \propto r^{-2}$. A steeper density profile was also discussed by Chandra et al. (2009), who argue for $\rho_w \propto r^{-2.6}$ for the last epochs discussed in their paper.

Since we do not include radiative cooling in the hydro-dynamic simulations, we have concentrated on epochs later than 1000 days (see also below). We show two cases, where the black line depicts the emission from the plasma shocked by the reverse shock and the red line exhibits the effect of clumping. For clumping, we assume that all of the gas shocked by the reverse shock is compressed further by a factor of three (and has a factor of three lower filling factor). It is considered in our model that the gas is in pressure equilibrium, so that the temperature of the compressed plasma is a factor of three lower than for the original model. As can be seen in Figure 8, our model simulates the emission fine for the light curve of soft X-ray emission up to ~ 7000 days, without invoking any type of clumping of the shocked ejecta (solid black line). Including an extra compression by a factor of 3 increases the soft X-ray

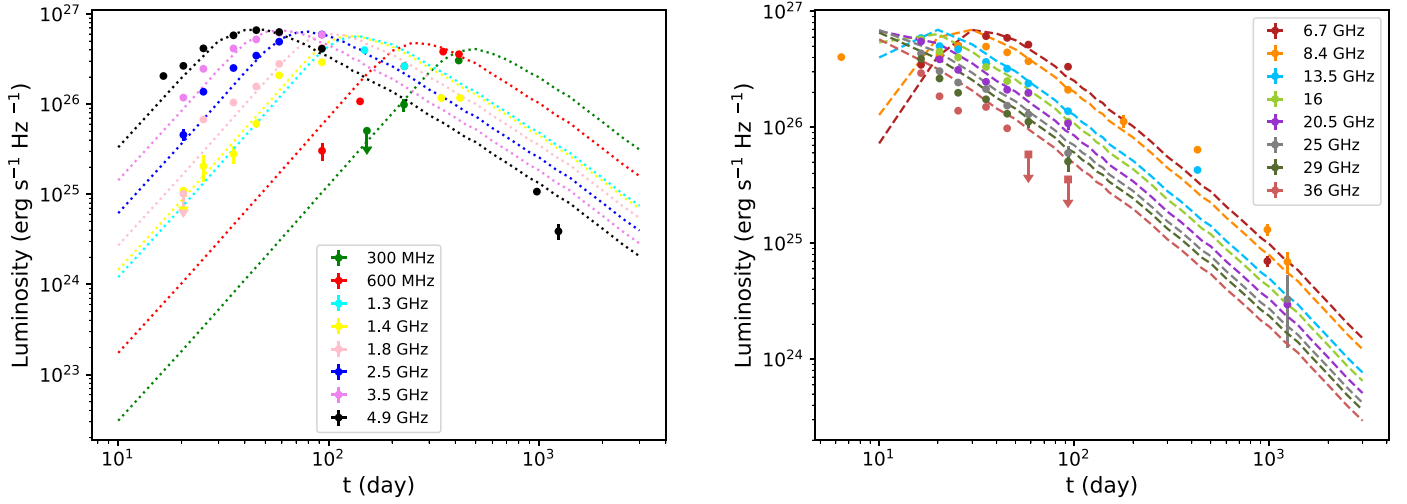


Figure 7. Radio light curves of SN 2011dh in the range 300 MHz to 4.9 GHz (left-hand panel) and between 6.7 GHz and 36 GHz (right-hand panel) for a wind-like ambient medium characterized by $\dot{M} = 4 \times 10^{-6} M_{\odot} \text{ yr}^{-1}$ and $v_w = 10 \text{ km s}^{-1}$. The data are from Soderberg et al. (2012), Krauss et al. (2012), de Witt et al. (2016) and this work. At high frequencies (right-hand panel), our model has overpredicted the emission at early epochs. The reason for this overestimate is that we did not consider inverse Compton cooling in our model because we are interested in studying the emission at late epochs. See the text for details.

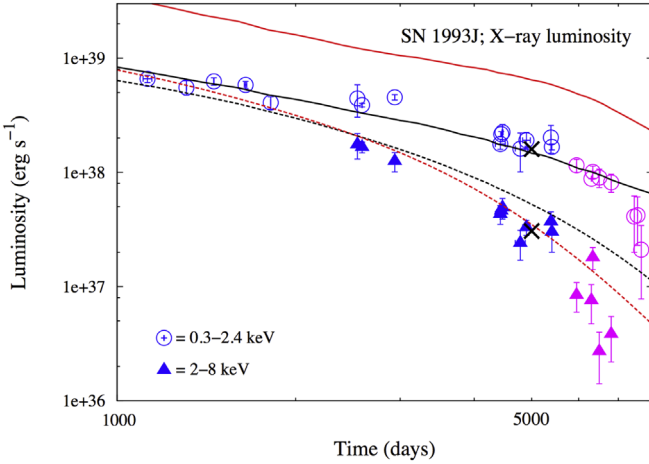


Figure 8. Modeled X-ray light curves for SN 1993J. Data in blue are from Chandra et al. (2009) and the data in magenta are from Dwarkadas et al. (2014). The solid black line is for the 0.3–2.4 keV emission and the solid red line is used for the same energy range, but assuming a factor of 3 extra compression of the shocked ejecta. The dashed black and red lines are the corresponding light curves for the 2–8 keV range. Note the relative insensitivity in emission due to this clumping effect for the 2–8 keV range. The two black crosses at 5000 days mark the effect of unequal temperatures of ions and electrons. These crosses relate to the black lines, but for the crosses we have put a cap on the electron temperature corresponding to 25% of the shock temperature. Whereas the model can adequately fit the light curves up to ~ 7000 days, the apparent faster downturn thereafter is not modeled well. A likely explanation for this is a flatter ejecta structure encountered by the reverse shock than in the model simulations (see the text).

emission significantly. Although clumping is, from many perspectives, much more complicated than just applying a compression factor, this gives a hint on how the emission can be affected by clumping (also see Figure 10, which demonstrates the impact of clumping on the X-ray spectrum). For the hard X-ray emission, the difference between the two models (i.e., no extra compression, and an extra factor-of-three compression) is small. Therefore, the variations in the soft X-ray light curve between 1000 and 3000 days could be due to modest density inhomogeneities at the reverse shock, rather

than invoking variations of the circumstellar density with radius, as was suggested by Chandra et al. (2009). A circumstellar density drop coinciding in radius with $r_s \sim 2 \times 10^{17} \text{ cm}$ may be needed, but the shallower ejecta profile encountered by the reverse shock also plays a role.

If t_{cool} and t_{dyn} represent the cooling and dynamic timescales, respectively, then our assumption of an adiabatic reverse shock for SN 1993J is justified by $t_{\text{cool}}/t_{\text{dyn}} > 1$ of newly shocked ejecta at all our epochs ($t > 1000$ days), even if an extra compression factor of 3 is added. If we do not add any extra compression, then the same is true for the full shock structure all the way out to the contact discontinuity. For the extra compression of 3, $t_{\text{cool}}/t_{\text{dyn}} < 1$ for the shocked ejecta closest to the contact discontinuity for all epochs considered here (i.e., up to 8000 days). Since Figure 8 indicates that no significant clumping is needed, we believe that an adiabatic shock structure is adequate. While the soft X-ray luminosity agrees reasonably well with observations out to ~ 7000 days, the emission from hard X-rays is overproduced in our model. This is most likely not an effect of clumping but could be due to unequal electron and ion temperatures (T_e and T_i , respectively). For example, at 5000 days, our simulations give a reverse shock temperature which is in the range $(0.7\text{--}6.1) \times 10^7 \text{ K}$. Limiting T_e so that it instead is in the range $(0.7\text{--}1.5) \times 10^7 \text{ K}$, decreases the hard X-ray flux by a factor of ~ 1.7 , while the soft X-ray flux is increased by $\sim 3\%$. This is shown with black crosses in Figure 8, and argues for $T_e/T_i \sim 0.25$ at the reverse shock, which is in line with the assumption of $T_e/T_i \sim 0.15$ by Chandra et al. (2009) to produce hard X-ray emission at adequate levels. For SN 1993J at 5000 days, in our model, the reverse shock is driven into helium-dominated ejecta and the equipartition timescale due to Coulomb collisions is $t_{\text{eq}} \sim 3.4 \times 10^3 (T_e/10^7 \text{ K})^{3/2} (n_{\text{He}}/10^3 \text{ cm}^{-3})^{-1} \text{ days}$ (Spitzer 1964). In our model, the helium density is $\sim 4.1 \times 10^3 \text{ cm}^{-3}$ ($1.2 \times 10^3 \text{ cm}^{-3}$) at 5000 (8000) days, so that $t_{\text{eq}} < t_{\text{dyn}}$. This is shown in Figure 9. While Coulomb collisions are unable to fully equilibrate ion and electron temperatures at the shock front, a ratio of $T_e/T_i = 0.15$ seems to be on the low side, unless the ejecta density is lower than in our model. This could be the case if the slope of the ejecta profile is flatter than in our

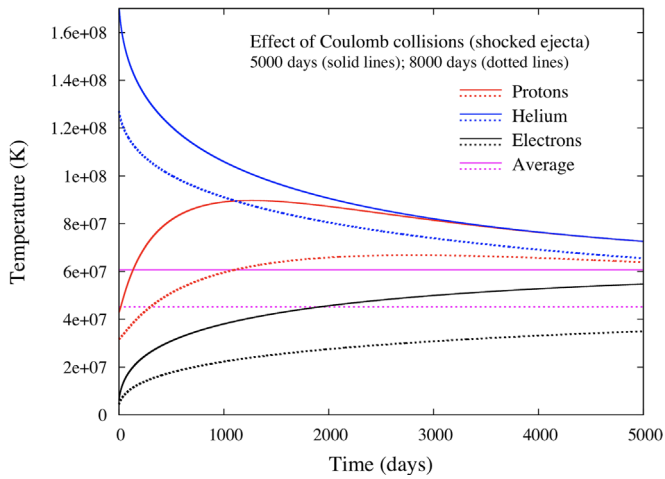


Figure 9. Temperatures for a fully ionized H-He plasma, simulating the shocked ejecta of SN 1993J at 5000 days (solid lines) and 8000 days (dotted lines). Blue represents helium, red represents protons and black represents electrons. Only Coulomb collisions are considered, except for electrons which are assumed to attain 10% of the average shock temperature immediately behind the shock front. Density and abundances are assumed to be constant with time since the gas was shocked. At these epochs, the He/H-ratio (by number) in our simulation of SN 1993J is ~ 38 and ~ 94 , respectively. Note the long time for temperature equilibration of electrons and ions.

model at these epochs. The positions of the reverse shock in our ejecta model at 1000, 2000, 3000, 5000, 7000 and 8000 days are shown with dotted lines in the left-hand panel of Figure 1.

7.2.2. SN 2011dh

For SN 2011dh, Figure 10 shows our modeled X-ray emission at 500 days for a wind characterized by a mass-loss rate of $4 \times 10^{-6} (v_w/10 \text{ km s}^{-1}) M_\odot \text{ yr}^{-1}$. As for SN 1993J, we consider two cases, where the spectrum in red exhibits the emission from the shocked ejecta without assuming a compression factor. The spectrum is featureless and dominated by free-free emission, as expected given the high temperature of the shocked ejecta, $\sim 3.5 \times 10^8$ K. The black spectrum in Figure 10 shows the effect of clumping. This figure demonstrates that clumping influences the spectrum at energies below ~ 2 keV. This is the reason why, in case of SN 1993J, we see small differences in hard X-ray luminosity (2–8 keV) calculated without considering any compression and invoking a clumping of a factor of 3 (black- and red-dashed lines in Figure 8).

Clumping decreases the cooling time, t_{cool} , of the shocked gas, which makes it more likely to become shorter than the dynamical timescale, t_{dyn} . Looking into the two compression factors (i.e., 1 and 3) in the models in Figure 10 in more detail, t_{cool} of the just shocked ejecta is $\sim 9.9 \times 10^5$ days and $\sim 1.9 \times 10^5$ days, respectively. Since t_{dyn} is 500 days, this means that shocks driven into the ejecta are not radiative, which justifies our model assumption of an adiabatic shock. This does not necessarily mean that radiative cooling could not affect the shock structure. Close to the contact discontinuity, the cooling times are $\sim 1.5 \times 10^3$ days and $\sim 1.3 \times 10^2$ days, respectively. This means that for the factor-of-3-compressed model, radiative cooling close to the contact discontinuity

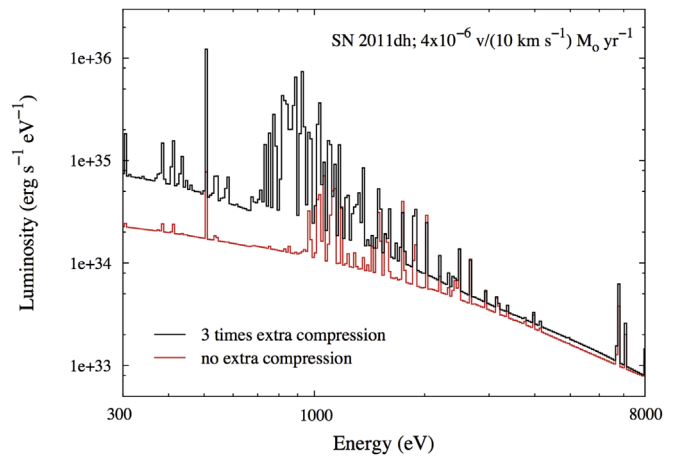


Figure 10. Modeled X-ray emission from SN 2011dh at 500 days after explosion. The spectrum in red comes from the reverse shock using parameters from our hydro models. The spectrum in black is for an assumed extra compression of the shocked ejecta by a factor of three, considering pressure equilibrium. This gives an indication of the effect of clumping in the shocked ejecta. Note that the spectra above ~ 2 keV are very similar.

(where the temperature falls below $\sim 10^7$ K) could marginally affect the modeled spectrum.

For the two clump compression factors, 1 and 3, the post-processed spectral synthesis using our adiabatic models gives luminosities from the reverse shock that are $\sim 6.3 \times 10^{37} \text{ erg s}^{-1}$ and $\sim 2.1 \times 10^{38} \text{ erg s}^{-1}$, respectively. This is much less than for a fully radiative reverse shock, $L_{\text{rev}} = 2\pi r_{\text{ej}}^2 \rho_{\text{ej}} v_{\text{rev}}^3$, which for our SN 2011dh model at 500 days is $\sim 1.0 \times 10^{40} \text{ erg s}^{-1}$. Here r_{ej} and ρ_{ej} represent the radius and density of the outermost unshocked ejecta, respectively; and v_{rev} is the reverse shock velocity. This estimate indeed shows that radiative cooling is not important for the reverse shock of SN 2011dh at 500 days. In the range 0.3–8.0 keV the luminosities are $\sim 4.1 \times 10^{37} \text{ erg s}^{-1}$ and $\sim 1.5 \times 10^{38} \text{ erg s}^{-1}$ for the compression factors 1 and 3, respectively. The observed luminosity in the range 0.3–8.0 keV is $\sim 6 \times 10^{37} \text{ erg s}^{-1}$ (Maeda et al. 2014), which indicates that only modest clumping of the gas being shocked is needed for our model with $4 \times 10^{-6} (v_w/10 \text{ km s}^{-1}) M_\odot \text{ yr}^{-1}$ to reproduce the observed emission. The analysis by Maeda et al. (2014) suggested a wind density roughly half that in our analysis. This difference stems from an assumed high power-law index, $n = 20$, for the density of the supernova ejecta, $\rho_{\text{ej}} \propto r^{-n}$, in Maeda et al. (2014). In the self-similar solution (Chevalier 1982), $\rho_{\text{ej}}/\rho_{\text{csm}}$ is a strong function of n . In our model, $n \approx 7$ around 500 days. However, the structure of the shocked ejecta has a memory of a much steeper profile of the outermost ejecta being shocked at earlier times (see right-hand panel of Figure 1). The position of the reverse shock in our ejecta model at 500 days, along with that at epochs 200 and 1200, is shown with a dotted line in the right-hand panel of Figure 1.

8. Discussion: Binary Evolution of Progenitors

The progenitors of SNe 1993J and 2011dh were very likely to have been part of a binary system. Although the binary companion of SN 1993J has not yet been discovered exclusively, many studies carried out during the last 25 yr (Nomoto et al. 1993; Podsiadlowski et al. 1993; Aldering et al. 1994; Cohen et al. 1995;

Maund et al. 2004; Maund & Smartt 2009; Fox et al. 2014) have pointed toward the presence of a massive hot companion star in the vicinity of the SN. The proposed model for the SN 1993J progenitor system consists of two stars of comparable masses, $\sim 15 M_{\odot}$ each (Nomoto et al. 1993; Podsiadlowski et al. 1993; Maund et al. 2004), and in which the progenitor star loses mass to the binary companion through the stable case C mass transfer (Podsiadlowski et al. 1992). After the exhaustion of the core helium, when the progenitor is on the asymptotic giant branch, the primary fills its Roche lobe and starts to transfer mass to the companion. The secondary accretes most of the transferred material and the remaining fraction gets lost in the surrounding medium. The mass transfer ceases when the primary has transferred nearly all of its hydrogen envelope. At this point, the hydrogen mass in the envelope of the primary becomes less than a certain level and the star starts to shrink. Consequently, it is now not possible for the primary to fill its Roche lobe. The primary then slowly loses the residual hydrogen envelope through stellar winds. For a $\sim 0.5 M_{\odot}$ residual envelope mass, and a mass-loss rate of $4 \times 10^{-5} M_{\odot} \text{ yr}^{-1}$, it will take around $12 \times 10^3 \text{ yr}$ to completely strip the envelope. This time is enough for the evolved star to go off as SN.

From our radio and X-ray studies, we have indications that around 6500 yr before the explosion of SN 1993J, the density of the surrounding medium started to increase rapidly toward the time leading up to the explosion. This implies that before $\sim 10^4 \text{ yr}$ prior the explosion, the mass-loss mechanism was most likely different from that due to the wind from the primary star. It is possible that before this time the primary mainly loses mass to the secondary companion through Roche lobe overflow and because of the high accretion efficiency of the companion, a very small percentage of the accreted material was managed to escape from the system. For a star of main-sequence mass of $\sim 15 M_{\odot}$ the central carbon burning phase starts around $\sim 10^4 \text{ yr}$ prior the explosion. Therefore, it is possible that the primary ceases the mass transfer through Roche lobe overflow from the time that the carbon at the core starts to fuse. However, according to the Woosley et al. (1994), at the time of the explosion, the primary was big enough to be able to transfer mass to the secondary star through Roche lobe overflow. If this is the case, then it suggests that the accretion efficiency of the companion star decreases at the onset of the core carbon burning phase. Consequently, more mass gets lost in to the circumbinary medium and a comparatively dense ambient medium forms. It is, however, difficult to explain what exactly causes the accretion efficiency to change so abruptly around $t \sim 10^4 \text{ yr}$ prior to the explosion.

There exists another possibility. Maund et al. (2004) found that the binary companion of SN 1993J was very likely to be a B2 Ia star. For this kind of star, the mass-loss rate is in the range $(0.25-1) \times 10^{-6} M_{\odot} \text{ yr}^{-1}$ for a wind velocity of $\sim 600 \text{ km s}^{-1}$ (Kudritzki et al. 1999; Crowther et al. 2006). In our model, we assumed that the density of the surrounding medium for $t \ll 10^4 \text{ yr}$ (i.e., $r > 2 \times 10^{18} \text{ cm}$ ($\equiv R_{\text{out}}$)) can be characterized by $\dot{M} = 1.2 \times 10^{-5} M_{\odot} \text{ yr}^{-1}$ for a wind velocity of 600 km s^{-1} (i.e., $\dot{M} = 2 \times 10^{-7} M_{\odot} \text{ yr}^{-1}$ for $v_w = 10 \text{ km s}^{-1}$), which is around 25 times higher than that expect from a B2 Ia star. However, the derived \dot{M} and v_w for these stars are not independent of theoretical assumptions. It is found from our study that around 25 yr after the explosion, the radius of the SN is $\sim 9.4 \times 10^{17} \text{ cm}$. To probe a region beyond R_{out} , the SN will take another $\sim 25 \text{ yr}$. It is therefore possible that the

density around R_{out} is lower than what we have presumed in our model, and it is due to the winds from the companion star. Thus, the CSM before the carbon burning phase of the primary could have been created by the winds from the companion star and that from carbon burning until the explosion had been due to the mass loss through Roche lobe which gave rise to a comparatively dense surroundings.

In case of SN 2011dh, a YSG star was observed at the SN location in the pre-explosion *HST* archival imaging (Van Dyk et al. 2011). However, it was initially thought that the YSG was not the star that exploded but was rather a neighboring or companion of the progenitor (Arcavi et al. 2011; Van Dyk et al. 2011; Soderberg et al. 2012). Later, Van Dyk et al. (2013) conducted a search for the companion star of SN 2011dh ~ 650 days after the explosion using the *HST* WFC3, and found that the YSG had disappeared from the SN location. This implied that it was the supergiant that exploded and resulted in a type IIb SN. From optical and near-infrared photometry and spectroscopy of the SN, at early and late epochs, and modeling of the light curves, Ergon et al. (2014, 2015) suggested that SN 2011dh was part of a binary system. It is interesting that by analyzing *HST* data, Maund et al. (2015) and Folatelli et al. (2014) have detected a point like object, at all wavelengths, at the location of the SN.

From our study, we found that the radio and the X-ray emission from SN 2011dh is consistent with a wind medium (see Figure 7) characterized by a mass-loss rate of $4 \times 10^{-6} M_{\odot} \text{ yr}^{-1}$ for a wind velocity of 10 km s^{-1} . This value of \dot{M}/v_w is almost 10 times higher than that predicted by Soderberg et al. (2012) and Krauss et al. (2012) by analyzing the early radio and X-ray light curves. However, to explain the thermal X-ray emission at around ~ 500 days post-explosion (Maeda et al. 2014) it was necessary to adopt a high density medium with a $\dot{M} \sim 3 \times 10^{-6} M_{\odot} \text{ yr}^{-1} (v_w/20 \text{ km s}^{-1})^{-1}$ around the progenitor. As mentioned in Section 7.2.2, this estimate depends on the density slope of the ejecta model used, and we argued that our results and those of Maeda et al. (2014) are consistent. A likely reason for the difference between our work and Soderberg et al. (2012) and Krauss et al. (2012) is the high values of ϵ_B and ϵ_e used in the studies of those authors.

A star usually spends $\sim 3000 \text{ yr}$ in the YSG phase (Drout et al. 2009) before exploding. The mass-loss rate at this phase is highly unconstrained. Georgy (2011) carried out calculations of a single $\sim 14 M_{\odot}$ rotating stellar model and assumed a 3–10 times higher mass loss from the stars at the red supergiant (RSG) phase. It was demonstrated in this study that with a higher value of \dot{M} , the stars end their nuclear life at a position in the Hertzsprung-Russell diagram, which is roughly consistent with the observed position of several YSG progenitors. Therefore, it may be possible that SN 2011dh was an explosion of a YSG that was not a part of a binary system and which had undergone mass loss through wind at a high rate during its RSG phase, so that it had lost almost the entire hydrogen envelope before explosion. At present, it is not ruled out that a YSG in solitude could be responsible for SN 2011dh. However, it is difficult from our analysis to distinguish between the single and binary progenitor scenario. More observations in the near future may help to disentangle this issue.

For the radio emission of both SNe 1993J and 2011dh, VLBI radio imaging can give clues to the details of the circumstellar interaction. The details are best explored for SN 1993J. The radio images up to $\sim 10 \text{ yr}$ show that both the inner and outer edges of the radio shell expand roughly as $\propto t^m$,

with $m \simeq 0.85\text{--}0.87$ (Marcaide et al. 2009; Martí-Vidal et al. 2011b). We find $m \sim 0.85$ for this period, which is in agreement with the estimates by Marcaide et al. (2009) and Martí-Vidal et al. (2011b), while for epochs after ~ 2500 days, the reverse shock slightly lags behind this expansion and the forward shock speeds up. The former is due to the ejecta density slope being shallower at the position of the reverse shock. The latter is because of the sharp density decrease in the CSM. At ~ 5000 days, the reverse shock encounters ejecta with $n \sim 2.5$. We will explore this point and its ramifications for radio and X-ray emission in greater detail in future analyses. A discussion of how the radio emission may depend on the effects of a weakening reverse shock can be found in Björnsson (2015).

9. Conclusions

We have performed hydrodynamical simulations of the interaction between SN ejecta and the CSM. The SNe that we have modeled are SNe 1993J and 2011dh. For our study, we have taken the ejecta structures of these two SNe from numerical simulations (STELLA). The main aim of our study is to try to trace the mass-loss history of the progenitors, and hence gain information about the evolution of the progenitor systems. SN shocks are often bright in radio and X-ray wavelengths. While the radio emission has been assumed to mainly originate at the region close to the forward shock, the X-rays at late epochs predominantly come from the shocked ejecta behind the reverse shock. However, there is considerable uncertainty regarding the exact location of the radio emission, and VLBI imaging of SN 1993J actually shows a rather even distribution of radio emission for the full region between the two shocks. We have adopted this approach; i.e., we assume homogeneous radio emission from the shocked CSM. For the X-rays, we assume that the sole produced is the reverse shock. Although radio and X-ray emission emanate from different parts of the shocked gas, the flux of both depends on the density and the structure of the surrounding medium, and also on the slope of the density profile of the SN ejecta. The density of the surrounding medium depends on the amount of mass ejected by the progenitor system during its evolution. Therefore, the mass-loss rates from the progenitor system at different phases of its evolution can be mapped with accurate information about the evolution of SN shocks, a reliable ejecta model, and proper modeling of radio and X-ray emissions.

The late time radio and X-ray curves of SN 1993J have shown a sudden downturn in radio and X-ray fluxes beyond ~ 3000 days after the explosion of the SN. In addition, the inner edge of the radio shell starts to lag compared to the $\propto t^{0.85}$ evolution at earlier epochs. By evaluating the SN evolution through hydro-simulation, and studying late time radio and X-ray emissions from SN 1993J, we found that to account for the observed drops, the density of the CSM needs to decrease rapidly at $r > 2 \times 10^{17}$ cm. For smaller radii, the wind density is characterized by $\dot{M} = 4 \times 10^{-5} M_{\odot} \text{ yr}^{-1}$ for $v_w = 10 \text{ km s}^{-1}$. This implies that if the primary transfers mass to the companion through Roche lobe overflow from the end of the core helium burning stage until the explosion, then $\sim 6500 (v_w/10 \text{ km s}^{-1})^{-1} \text{ yr}$ before the explosion the accretion efficiency of the secondary decreases. Therefore, more mass gets ejected in the ambient medium, which makes it denser. For a primary, with a $\sim 15 M_{\odot}$ main-sequence mass, it is expected that around 10^4 yr prior to the explosion, the star was burning

the carbon present in its core. However, figuring out the reason behind this decrease in accretion efficiency of the companion star is beyond the scope of this paper.

An important future investigation is to test the scenario discussed by Björnsson (2015), who suggests that the seemingly achromatic break in radio and X-ray light curves around ~ 3000 days could be due to the reverse shock entering a flat part of the ejecta density profile. When this happens, the reverse shock would weaken, or perhaps even disappear. This should reduce the X-ray emission and cause a decline in the radio emission. In our model, the density profile of the ejecta just about to be shocked around 3000 days is $n = 3.1$. In the scenario envisioned by Björnsson, the density profile is even shallower. This would produce weaker X-ray emissions than in our model and could be a reason why our X-ray light curves in Figure 8 overshoot at $t > 5000$ days.

In the case of SN 2011dh, both radio and X-ray emissions are consistent with a wind-like ambient medium. From *HST* WFC3 imaging around 650 days after the explosion, Van Dyk et al. (2013) confirm that the YSG discovered in the pre-explosion archival *HST* image was the progenitor of the SN. With the SN ejecta structure from STELLA, we found that to account for both the radio and the X-ray fluxes at late time we require $\dot{M} = 4 \times 10^{-6} M_{\odot} \text{ yr}^{-1}$ for $v_w = 10 \text{ km s}^{-1}$. It is, however, difficult from our study to conclude whether the YSG had evolved in solitude or was a part of a binary system. Nevertheless, in future, if we observe a drop in radio and X-ray emission from SN 2011dh, similar to that observed from SN 1993J, then this would suggest a scenario where the progenitors of both SNe 1993J and 2011dh had undergone a similar binary evolution before explosion.

We thank Claes-Ingvar Björnsson, Michiel Buisraan and Claes Fransson for our discussions. The software used in this work was in part developed by the DOE NNSA-ASC OASCR Flash Center at the University of Chicago. The hydrodynamical simulations shown were performed on resources provided by the Swedish National Infrastructure for Computing (SNIC) at PDC (Beskow), Royal Institute of Technology, Stockholm. P.C. acknowledges support from the Department of Science and Technology via the SwaranaJayanti Fellowship award (file No. DST/SJF/PSA-01/2014-15).

ORCID iDs

E. Kundu  <https://orcid.org/0000-0002-4807-379X>

P. Lundqvist  <https://orcid.org/0000-0002-3664-8082>

References

- Aldering, G., Humphreys, R. M., & Richmond, M. 1994, *AJ*, 107, 662
- Arcavi, I., Gal-Yam, A., Polishook, D., et al. 2011, *ATel*, 3413, 1
- Arcavi, I., Gal-Yam, A., Yaron, O., et al. 2011, *ApJL*, 742, L18
- Bartel, N., Bietenholz, M. F., Rupen, M. P., et al. 2000, *Sci*, 287, 112
- Bartel, N., Bietenholz, M. F., Rupen, M. P., et al. 2002, *ApJ*, 581, 404
- Bietenholz, M. F., Brunthaler, A., Soderberg, A. M., et al. 2012, *ApJ*, 751, 125
- Björnsson, C.-I. 2015, *ApJ*, 813, 43
- Björnsson, C.-I., & Lundqvist, P. 2014, *ApJ*, 787, 143
- Blinnikov, S., Lundqvist, P., Bartunov, O., Nomoto, K., & Iwamoto, K. 2000, *ApJ*, 532, 1132
- Blinnikov, S. I., Eastman, R., Bartunov, O. S., Popolitov, V. A., & Woosley, S. E. 1998, *ApJ*, 496, 454
- Blinnikov, S. I., Röpke, F. K., Sorokina, E. I., et al. 2006, *A&A*, 453, 229
- Bykov, A. M., Brandenburg, A., Malkov, M. A., & Osipov, S. M. 2013, *SSRv*, 178, 201
- Campana, S., & Immler, S. 2012, *MNRAS*, 427, L70
- Caprioli, D., & Spitkovsky, A. 2014a, *ApJ*, 783, 91

- Caprioli, D., & Spitkovsky, A. 2014b, *ApJ*, 794, 46
- Chandra, P., Dwarkadas, V. V., Ray, A., et al. 2009, *ApJ*, 699, 388
- Chandra, P., Ray, A., & Bhatnagar, S. 2004, *ApJ*, 612, 974
- Chandra, P., Ray, A., Schlegel, E. M., Sutaria, F. K., & Pietsch, W. 2005, *ApJ*, 629, 933
- Chevalier, R. A. 1982, *ApJ*, 258, 790
- Cohen, J. G., Darling, J., & Porter, A. 1995, *AJ*, 110, 308
- Colella, P., & Woodward, P. 1984, *JCoPh*, 54, 174
- Crockett, R. M., Eldridge, J. J., Smartt, S. J., et al. 2008, *MNRAS*, 391, L5
- Crowther, P. A., Lennon, D. J., & Walborn, N. R. 2006, *A&A*, 446, 279
- de Witt, A., Bietenholz, M. F., Kamble, A., et al. 2016, *MNRAS*, 455, 511
- Drout, M. R., Massey, P., Meynet, G., Tokarz, S., & Caldwell, N. 2009, *ApJ*, 703, 441
- Dwarkadas, V. V., Bauer, F., Bietenholz, M., & Bartel, N. 2014, in *The X-ray Universe 2014*, ed. J.-U. Ness, 248, <http://www.cosmos.esa.int/web/xmm-newton/2014-symposium/>
- Ergon, M., Jerkstrand, A., Sollerman, J., et al. 2015, *A&A*, 580, A142
- Ergon, M., Sollerman, J., Fraser, M., et al. 2014, *A&A*, 562, A17
- Feldmeier, J. J., Ciardullo, R., & Jacoby, G. H. 1997, *ApJ*, 479, 231
- Filippenko, A. V. 1997, *ARA&A*, 35, 309
- Folatelli, G., Bersten, M. C., Benvenuto, O. G., et al. 2014, *ApJL*, 793, L22
- Fox, O. D., Bostroem, K. A., Van Dyk, S. D., et al. 2014, *ApJ*, 790, 17
- Fransson, C., & Björnsson, C.-I. 1998, *ApJ*, 509, 861
- Fransson, C., Lundqvist, P., & Chevalier, R. A. 1996, *ApJ*, 461, 993
- Freedman, W. L., Hughes, S. M., Madore, B. F., et al. 1994, *ApJ*, 427, 628
- Fryxell, B., Olson, K., Ricker, P., et al. 2000, *ApJS*, 131, 273
- Fryxell, B. A., Müller, E., & Arnett, D. 1989, *Hydrodynamics and Nuclear Burning*, MPI Astrophys. Rep. 449 (Garching: MPI Astrophys.)
- Georgy, C. 2011, *A&A*, 538, L8
- Harten, A., Lax, P., & van Leer, B. 1983, *SIAMR*, 25, 35
- Immler, S., Aschenbach, B., & Wang, Q. D. 2001, *ApJL*, 561, L107
- Kohmura, Y., Inoue, H., Aoki, T., et al. 1994, *PASJ*, 46, L157
- Krauss, M. I., Soderberg, A. M., Chomiuk, L., et al. 2012, *ApJL*, 750, L40
- Kudritzki, R. P., Puls, J., Lennon, D. J., et al. 1999, *A&A*, 350, 970
- Kundu, E., Lundqvist, P., Pérez-Torres, M. A., et al. 2017, *ApJ*, 842, 17
- Maeda, K., Katsuda, S., Bamba, A., et al. 2014, *ApJ*, 785, 95
- Marcaide, J. M., Alberdi, A., Ros, E., et al. 1995a, *Sci*, 270, 1475
- Marcaide, J. M., Alberdi, A., Ros, E., et al. 1995b, *Natur*, 373, 44
- Marcaide, J. M., Alberdi, A., Ros, E., et al. 1997, *ApJL*, 486, L31
- Marcaide, J. M., Martí-Vidal, I., Alberdi, A., et al. 2009, *A&A*, 505, 927
- Marion, G. H., Kirshner, R., Wheeler, J. C., et al. 2011, *ATel*, 3435, 1
- Martí-Vidal, I., Marcaide, J. M., Alberdi, A., et al. 2011a, *A&A*, 526, 142
- Martí-Vidal, I., Tudose, V., Paragi, Z., et al. 2011b, *A&A*, 535, L10
- Mattila, S., Meikle, W. P. S., Lundqvist, P., et al. 2008, *MNRAS*, 389, 141
- Maund, J. R., Arcavi, I., Ergon, M., et al. 2015, *MNRAS*, 454, 2580
- Maund, J. R., Fraser, M., Ergon, M., et al. 2011, *ApJL*, 739, L37
- Maund, J. R., & Smartt, S. J. 2009, *Sci*, 324, 486
- Maund, J. R., Smartt, S. J., Kudritzki, R. P., Podsiadlowski, P., & Gilmore, G. F. 2004, *Natur*, 427, 129
- McMullin, J. P., Waters, B., Schiebel, D., Young, W., & Golap, K. 2007, in *ASP Conf. Ser. 376, Astronomical Data Analysis Software and Systems XVI*, ed. R. A. Shaw, F. Hill, & D. J. Bell (San Francisco, CA: ASP), 127
- Nomoto, K., Suzuki, T., Shigeyama, T., et al. 1993, *Natur*, 364, 507
- Nymark, T. K., Fransson, C., & Kozma, C. 2006, *A&A*, 449, 171
- Osterbrock, D. E. 1989, *Astrophysics of Gaseous Nebulae and Active Galactic Nuclei* (Mill Valley, CA: Univ. Science Books)
- Pérez-Torres, M. A., Alberdi, A., & Marcaide, J. M. 2001, *A&A*, 374, 997
- Pérez-Torres, M. A., Alberdi, A., & Marcaide, J. M. 2002, *A&A*, 394, 71
- Podsiadlowski, P. 2001, in *Accretion Process in Astrophysics*, ed. I. G. Martínez-Pais, T. Shahbaz, & J. C. Velazquez (Cambridge: Cambridge Univ. Press), 45
- Podsiadlowski, P., Hsu, J. J. L., Joss, P. C., & Ross, R. R. 1993, *Natur*, 364, 509
- Podsiadlowski, P., Joss, P. C., & Hsu, J. J. L. 1992, *ApJ*, 391, 246
- Pooley, G. G., & Green, D. A. 1993, *MNRAS*, 264, L17
- Rybicki, G. B., & Lightman, A. P. 1979, *Radiative Processes in Astrophysics* (New York: Wiley-Interscience)
- Schaller, G., Schaerer, D., Meynet, G., & Maeder, A. 1992, *A&AS*, 96, 269
- Smartt, S. J. 2015, *PASA*, 32, e016
- Smith, N., Li, W., Filippenko, A. V., & Chornock, R. 2011, *MNRAS*, 412, 1522
- Smith, N., & Owocki, S. P. 2006, *ApJL*, 645, L45
- Soderberg, A. M., Margutti, R., Zauderer, B. A., et al. 2012, *ApJ*, 752, 78
- Sorokina, E. I., Blinnikov, S. I., Kosenko, D. I., & Lundqvist, P. 2004, *AstL*, 30, 737
- Spitzer, L., Jr. 1964, *Physics of Fully Ionized Gases* (New York: Wiley)
- Swartz, D. A., Ghosh, K. K., McCollough, M. L., et al. 2003, *ApJS*, 144, 213
- Tsvetkov, D. Y., Volkov, I. M., Sorokina, E. I., et al. 2012, *PZ*, 32, 6
- Tucker, W. 1975, *Radiation Processes in Astrophysics* (Cambridge, MA: MIT Press)
- Uno, S., Mitsuda, K., Inoue, H., et al. 2002, *ApJ*, 565, 419
- Van Dyk, S. D., Li, W., Cenko, S. B., et al. 2011, *ApJL*, 741, L28
- Van Dyk, S. D., Li, W., Zheng, W. K., et al. 2013, *ApJL*, 772, L32
- van Dyk, S. D., Weiler, K. W., Sramek, R. A., Rupen, M. P., & Panagia, N. 1994, *ApJL*, 432, L115
- Van Dyk, S. D., Zheng, W., fox, O. D., et al. 2014, *ApJ*, 147, 37
- Vink, J. S., & Koter, A. de. 2005, *A&A*, 442, 587
- Weiler, K. W., Williams, C. L., Panagia, N., et al. 2007, *ApJ*, 671, 1959
- Woosley, S. E., Eastman, R. G., Weaver, T. A., & Pinto, P. A. 1994, *ApJ*, 429, 300
- Woosley, S. E., Kasen, D., Blinnikov, S., & Sorokina, E. 2007, *ApJ*, 662, 487
- Zimmermann, H.-U., & Aschenbach, B. 2003, *A&A*, 406, 969